Carbohydrate Polymers 348 (2025) 122887

Contents lists available at ScienceDirect

Carbohydrate Polymers

journal homepage: www.elsevier.com/locate/carbpol

Hemp cellulose-based aerogels and cryogels: From waste biomass to sustainable absorbent pads for food preservation

Laura Cabrera-Villamizar [a], Jéssica Fernanda Pereira [a], María Castanedo [a], Amparo López-Rubio [a,b], María José Fabra [a,b,*]

[a] Food Safety and Preservation Department, Institute of Agrochemistry and Food Technology (IATA), CSIC, Valencia, Spain
[b] Interdisciplinary Platform for Sustainable Plastics Towards a Circular Economy- Spanish National Research Council (SusPlast-CSIC), Madrid, Spain

ARTICLE INFO

Keywords:
Hemp cellulose
Aerogels
Cryogels
Absorbent pads
Food preservation

ABSTRACT

This study presents a circular economy approach utilizing hemp stems and rice straw, typically perceived as low-value agricultural waste, to develop a sustainable alternative to traditional plastic absorbent pads for food packaging. The development of an active material was achieved through the utilization of hemp cellulose and a bioactive extract isolated from rice straw. In addition to reducing plastic pollution, this material demonstrates the potential to enhance food preservation. This research provides evidence of the benefits of repurposing agricultural by-products to create valuable and environmentally-friendly products. Hemp cellulose was extracted, characterized, and processed to develop stable aerogels and cryogels through supercritical CO_2 drying and freeze-drying. The water stability and internal structure of the materials were guided via TEMPO-mediated oxidation and high-pressure homogenization. Both materials showed versatile physicochemical and mechanical properties. Nevertheless, with higher water sorption (2.20 mL/g), minimal dimensional changes, and lower shrinkage, cryogels were suitable for meat absorbent pad application. To enhance the cryogels functionality, they were impregnated with a rice straw bioactive extract in two different concentrations. The incorporation of the extract did not affect the structure of the cryogels, improved their mechanical properties and the antioxidant activity remained stable after drying (63.89–78.96 %). Finally, the performance of the developed materials was compared to commercial plastic pads and pristine meat preservation challenge test during 9 days at refrigeration conditions. The incorporation of rice straw extract improved meat color preservation. While moderate extract concentrations (75 mg/g) showed a protective effect against lipid oxidation, higher levels (187.5 mg/g) induced pro-oxidant reactions. This research highlights the potential of hemp cellulose-based cryogels as sustainable and functional packaging materials for meat products.

1. Introduction

Aerogels and cryogels are porous materials that can be prepared from organic, inorganic and even composites of different materials with a potential use for a wide range of applications, such as liquid sorption, thermal insulation, filtration and as carriers for different active molecules (Long et al., 2018). However, worries about sustainability, biodegradability and long-term environmental impact have driven research to find environmentally-friendly alternatives. In this regard, the use of biopolymers (i.e. polysaccharides, gums and proteins) has been gaining attention for aerogel preparation (Nita et al., 2020) due to their biodegradable, biocompatible and renewable characteristics.

Aerogels are materials with exceptional properties, including ultra-low density, high porosity and variable mechanical and thermal insulation depending on the composition. These characteristics make them highly versatile for diverse applications (Liebner et al., 2008). The drying method employed significantly influences the internal structure and functional properties of aerogels. Supercritical CO_2 drying (SC-CO_2) and freeze-drying are commonly used to produce aerogels and cryogels, respectively (Darpentigny et al., 2020). While SC-CO_2 drying offers advantages such as preserving the original gel structure, complete solvent removal, and a higher specific surface area, with smaller pore sizes suitable for controlled release, it comes with increased production costs and requires more processing steps to ensure hydrogel stability and

* Corresponding author at: Food Safety and Preservation Department, Institute of Agrochemistry and Food Technology (IATA), CSIC, Valencia, Spain.
E-mail addresses: la.cabrera10@iata.csic.es (L. Cabrera-Villamizar), jessicapereira@ufscar.br (J.F. Pereira), maria.castanedo@iata.csic.es (M. Castanedo), amparo.lopez@iata.csic.es (A. López-Rubio), mjfabra@iata.csic.es (M.J. Fabra).

https://doi.org/10.1016/j.carbpol.2024.122887
Received 3 September 2024; Received in revised form 14 October 2024; Accepted 15 October 2024
Available online 19 October 2024

solvent replacement (Yang & Cranston, 2014). In contrast, cryogels are characterized by lower production costs, higher mechanical strength, and faster compound release (Korhonen & Budtova, 2020). However, they exhibit lower specific surface area and may experience structural degradation due to ice crystal formation during the drying process (Buchtová et al., 2019). By investigating both SC-CO_2 drying and freeze-drying in the context of food-absorbent pad development, this study aims to explore their respective impacts and suitability for industrial applications.

Furthermore, the material from which they are made is of great importance in determining their applications. Polysaccharides and, in particular, lignocellulosic materials have already demonstrated their potential to develop aerogels (Benito-González et al., 2020; Benito-González et al., 2021; de Oliveira et al., 2019; Fontes-Candia et al., 2019; Zaman et al., 2020a). Cellulosic materials can be extracted from agro-industrial residues and forestry-derived waste by-products such as husks, leaves, stems and seeds (Vallejo et al., 2021), and the quality and properties of the obtained cellulose will be also influenced by its source and processing. One sustainable source of cellulose is hemp (*Cannabis sativa*) and its derivatives. Hemp cellulose possesses excellent mechanical properties, providing stiffness and strength to composite materials (Momeni et al., 2021). Furthermore, hemp is a more sustainable solution than other wood crops, as it is a fast-growing plant whose residues can be valorized (Ahmed et al., 2022). In addition, hemp cellulose has proven to be one of the best materials for papermaking due to its strength and lightness, ascribed to the facility to form an structural network and the presence of longer fibers than other plants, making it stronger (Gibson, 2006).

Previous reports have shown the production of cryogels from hemp cellulose for thermal insulation (Beluns et al., 2021; Zhu et al., 2023); oil sorption in seawater (Paulauskiene et al., 2024); controlled release of fertilizers (Kaur et al., 2023), and wastewater or air cleaning (Lyu et al., 2023). While previous studies have demonstrated the versatility of hemp cellulose cryogels in various applications, their potential for food-related uses, such as food preservation pads and SC-CO_2 drying techniques, remains unexplored. This research seeks to address this knowledge gap by investigating the feasibility and effectiveness of hemp-cellulose cryogels and aerogels in this specific context. In the particular case of meat packaging, non-permeable/non-stick synthetic polymers containing a hydrophilic non-woven bottom layer filled with active compounds (i.e., sodium bicarbonate or citric acid) are used to produce absorbing pads to use them as part of the packaging structure. They absorb the excess of liquids released upon food storage, improve the visual perception, prevent bacterial growth and other factors that could alter product quality (Castrica et al., 2020). To reduce environmental impact, research efforts are being focused on the use of more sustainable bio based and renewable materials (i.e., cellulose) to produce food-grade absorbing pads (Iskandar et al., 2022). Advantageously, porous cellulosic materials can be also impregnated with active compounds with proved antimicrobial/antioxidant properties to enhance food preservation performance (Fontes-Candia et al., 2019). For example, alternative approaches to the development of active antimicrobial aerogels have involved the incorporation of metals and their oxide nanoparticles, which can be safely incorporated into food packaging (Wu, Zhou, et al., 2023). Nevertheless, consumers and researchers tend to be more receptive to the utilization of plant-derived compounds. In the context of valorization of lignocellulosic waste in the transition to circular economy, Cabrera-Villamizar, Ebrahimi, et al. (2024) have recently developed greener strategies for rice straw biorefinery using combined alkali, ozone and enzyme treatments to obtain added-value by-products, not only cellulose-rich fractions but also valuable antioxidant compounds to develop active materials. Particularly, the alkaline fraction exhibited a high concentration of lignin derivatives and polyphenols. This bioactive extract, with antioxidant properties, is a promising candidate for developing bioactive materials while minimizing waste, reducing the use of synthetic additives, and meeting consumer demands for natural and plant-based products.

In the present work, hemp cellulose rich fractions were combined with the polyphenol-rich extract (the most important by-product obtained from rice straw biorefinery process) to obtain antioxidant absorbing pads. It is hypothesized that not only the drying conditions but also the composition of the active extract will affect the internal morphology and, thus, physicochemical and functional properties of the hemp cellulose-based aerogels/cryogels. Therefore, this work aimed at understanding how drying process (SC-CO_2 vs. freeze-drying) affected the physicochemical properties of hemp cellulose-based aerogels and how a side-stream, rich in polyphenols, obtained from rice straw biorefinery impacted on the functionality and properties of the developed absorbing pads for food packaging applications. Moreover, this study provides valuable insights into their impact on the materials structure and functionality. Additionally, the findings construct a baseline for development of sustainable effective absorbent pads using plant-based matrix and bioactives. By addressing the gap in hemp cellulose-based aerogel research and comparing the two drying methods, this study contributed to the development of sustainable and effective packaging solutions for the food industry. Furthermore, the proof-of-concept validation in beef storage demonstrates the real-world applicability of this innovative approach.

2. Materials and methods

2.1. Materials

The dry biomass used in the present study were hemp stems (*Cannabis sativa*), which were grown during 2022 in Spain (Burgos) and provided by a local converter.

All reagents used were of analytical grade, including: hexane (LabKem, 95 %), toluene (VWR Chemicals, ≥98 %), ethanol (PanReac AppliChem, 99.5 %), NaClO2 (Sigma-Aldrich, 80 %), glacial acetic acid (LabKem, 99.8 %), KOH (Sigma-Aldrich, 90 %), TEMPO (Sigma-Aldrich, 98 %), NaBr (Sigma-Aldrich, ≥99 %), NaClO sodium hypochlorite solution (Sigma-Aldrich, 10–15 %), NaOH (PanReac AppliChem, ≥98 %), NaCl (PanReac AppliChem, 99 %), HCl (LabKem, 37 %), citric acid (Sigma-Aldrich, ≥99.5 %), β-carotene (Sigma-Aldrich, ≥97 %), chloroform (Carlo Erba Reagents, 99.9 %), linoleic acid (Sigma-Aldrich, ≥99 %), Tween ® 40 (Sigma-Aldrich), butylated hydroxytoluene (Sigma-Aldrich, ≥99 %), potassium phosphate buffer (NaH2PO4 (Sigma-Aldrich, ≥99 %) and Na2HPO4 (Sigma-Aldrich, ≥99 %)), HCl (Sigma-Aldrich, 37 %), ethanolic propyl gallate (Sigma-Aldrich, ≥98 %), EDTA (Sigma-Aldrich, 99.4–100.6 %), silicone antifoaming liquid (PanReac AppliChem), 2-thiobarbituric acid (Sigma-Aldrich, ≥98 %).

2.2. Raw material characterization

The hemp stems were washed with tap water to remove any adhering dirt or debris and dried at room temperature for one week. The dried stems were subsequently milled twice with mesh sizes of 3 mm and 1.5 mm to obtain a homogeneous powder before their characterization. Specifically, lignin content was determined according to the standard method TAPPI T211 om-07. The monosaccharide composition was determined by anion exchange chromatography with pulsed amperometric detection (HPAEC-PAD) with an ICS-3000 system (Dionex, Thermo Scientific, USA) after sulfuric hydrolysis as described by Cabrera-Villamizar, Ebrahimi, et al. (2024). The lipid content was estimated following a Soxhlet extraction procedure, which involved the use of 5 g of raw material with 80 mL of hexane for 2 h (Soxtec 8000, Foss Analytics, Denmark) and the protein content was determined using the Kjeldahl method, which measures the total nitrogen content in the samples.

2.3. Cellulose extraction and characterization

Cellulose extraction was performed with slight modifications based on the method described by Martínez-Sanz et al. (2018). The method consisted of three main steps: i) Dewaxing with Soxhlet extraction, ii) Lignin removal using an oxidative treatment and iii) Hemicellulose removal by means of an alkaline treatment. Briefly, 7 g of milled hemp stems were subjected to a three-step Soxhlet extraction using Soxtec TM 8000 apparatus (Foss Analytics, Denmark) to remove waxes, lipids, and pigments. A 2:1 (v/v) mixture of toluene and ethanol (75 mL total volume) was used as extraction solvent. Each extraction cycle consisted of a 30-min boiling phase at 210 °C, a 1.5-h extraction phase and a 10-min solvent recovery step. The resulting fraction was placed in a fume hood to allow the solvent evaporation for 24 h, followed by drying at 60 °C until constant weight was achieved. Subsequently, the dewaxed biomass was placed into 700 mL of a solution of 1.4 % (w/v) ($NaCLO_2$) adjusted to pH 3 using glacial acetic acid and then heated to 70 °C. The reaction occurred under magnetic stirring at 200 rpm for 5 h. Then, the reaction was stopped using an ice bath, and the mixture was filtered using a 15 μm nylon cloth. The obtained fraction was washed with distilled water until neutrality. Finally, the obtained biomass was added to 400 mL of a 5 % (w/v) KOH solution. The treatment was performed under magnetic stirring at 200 rpm at room temperature for 24 h, followed by an additional 2 h at 90 °C. The reaction was stopped with an ice bath, and then it was filtered to recover the cellulosic extract and was washed until neutral. The obtained cellulose fraction was stored in a hydrogel format under refrigeration until further use.

The cellulose and hemicellulose concentration were determined by ion exchange chromatography, as described in Section 2.2. Additionally, the cellulosic material's thermal stability and decomposition patterns were analyzed by thermogravimetric analysis (TGA), and the identification of functional groups present in the sample was recorded using Fourier-transform infrared spectroscopy (FTIR) analysis.

2.4. Cellulose oxidation, homogenization, and conductimetric titration

Cellulose TEMPO-mediated oxidation was conducted according to Isogai et al. (2011). Subsequently, high-pressure homogenization and carboxyl group determination were performed as described by Cabrera-Villamizar, Campano, et al. (2024) with some modifications. Briefly, the cellulose was oxidized using a solution (1 mmol TEMPO and 10 mmol NaBr), followed by the addition of 10 g of cellulose-rich fraction. The oxidation was initiated by adding 50 mmol of NaClO while maintaining the pH at 10.0 with 0.5 M NaOH until the pH stabilized, indicating that the reaction was complete. The oxidized cellulose was then recovered through extensive washing with deionized water until a neutral pH was achieved, followed by filtration using a nylon cloth with a 15 μm pore size, and it was stored at 4 °C. To prepare cellulose nanofibers (CNF), a 1 % (w/v) dispersion of the oxidized cellulose was sonicated (Ultrasonic Processor UP400S, Hielscher, Germany). The suspension was placed in an ice bath, under continuous sonication with 300 W/cm^2 of acoustic power density and 175 μm of amplitude, until no visible clumps remained. The morphology of the cellulosic fibers was analyzed through confocal laser scanning microscopy (CLSM) and transmission electron microscopy (TEM) using a Nikon Eclipse 90i wide-field microscope (Nikon Corporation, Japan) and a TEM JEOL jem 1010 100 kV (JEOL Ltd., Japan), respectively. For the CLSM analysis, samples of the suspension (10 μL) were dyed with 0.01 % Calcofluor White. In preparation for TEM visualization, the samples were pre-stained with a 2 % uranyl acetate solution. The degree of oxidation was evaluated through conductimetric titration (Eutech Cond 6+, Thermo Scientific, USA). Briefly, 0.15 g of dried pulp was mixed with 5 mL of 0.01 M NaCl and deionized water to a final volume of 55 mL. The pH adjusted to 2.8 using 0.05 M HCl and then incremental additions of 0.1 mL of 0.05 M NaOH were made while measuring conductivity, continuing until a consistent increase was observed, which indicated complete deprotonation of carboxylic acid groups. The volume of NaOH consumed between the initial stable baseline and the inflection point in the conductivity curve reflected the concentration of these functional groups in the oxidized pulp sample (Sanchez-Salvador et al., 2022).

2.5. Fabrication of aerogels and cryogels

The oxidized and homogenized suspension was used to prepare aerogels and cryogels. To fabricate aerogels, 2 g of the suspension were poured into each well on a 12-well plate (diameter 15 mm, height 20 mm, volume 3.53 cm^3). Then, 2 mL of 0.5 M citric acid was added carefully to the suspension for 10 min as a cross-linking agent to induce gelation as previously reported by Wang and Kim (2022). Then, the hydrogels were washed with distilled water. Followed by a solvent exchange by immersing the hydrogels in absolute ethanol for 5 d, with a solvent exchange every 24 h. The alcogels were placed in a supercritical CO_2 (SC-CO_2) extractor (ExtrateX, France). The drying conditions were 121 bar (12.1 MPa) with a pressure increase ramp of 10 bar/min up to 80 L/min of CO_2 flow rate, at 70 °C, for 4 h (isotherm). Finally, the controlled temperature was turned off and the equipment was gradually depressurized at a rate of 1 bar/min (0.1 MPa/min). On the other hand, to obtain cryogels 2 g of the suspension were poured into each well on a 12-well plate. To remove dissolved air, the solution underwent a dry blotting step. Subsequently, the plate was subjected to ultra-freezing at −80 °C, followed by freeze-drying (LyoBeta, Telstar, USA).

A caliper was used to measure the diameter of each sample in triplicate to quantify the shrinkage of the materials in their production. The shrinkage was determined across the different states of the materials: liquid, alcogel, dried, and after water vapor sorption. The resulting materials were then stored in a desiccator until further analysis to minimize sample moisture uptake.

2.6. Rice straw extract preparation and incorporation

The rice straw was milled with 3 mm and 1.5 mm mesh. The grounded biomass was then subjected to mild alkali hydrolysis, according to Cabrera-Villamizar, Ebrahimi, et al. (2024). Briefly, the rice straw was immersed into a solution of 1 M NaOH at pH 13 for 3 h at 121 °C in an autoclave. Then, the material was filtered using a nylon cloth of 15-μm pore size. The liquid extract was recovered and freeze-dried. Finally, the extract was dialyzed for 5 d in distilled water, and the dialysate was changed twice daily to reduce the salt concentration while keeping the lignin-derived compounds.

The extract was incorporated before the drying process. Thus, the rice straw extract in powder was added in concentrations of 75, 100, and 187.5 mg/g into the oxidized-homogenized suspension. Then, the drying processes were replicated as the control materials, as described in Section 2.5.

2.7. Antioxidant capacity

The antioxidant capacity of the rice straw extract was determined using a modified method described by Olszowy and Dawidowicz (2016). Briefly, 4 mg of β-carotene were dissolved in 10 mL of chloroform. In a round-bottom flask, 50 mg of linoleic acid and 400 mg of Tween 40 were weighed. 2 mL of the β-carotene solution were added, and the chloroform was evaporated to dryness using a rotary evaporator. Subsequently, 50 mL of aerated distilled water was added to the flask, and the mixture was vigorously stirred. Samples were prepared in distilled water at a final concentration of 2 mg/mL. Butylhydroxytoluene (BHT) served as the positive control, prepared at a concentration of 2 mg/mL in absolute ethanol. Distilled water was used as the negative control. A 96-well plate was used for the assay. Aliquots of 10 μL of samples and controls were carefully dispensed into the wells, followed by the addition of 250 μL of the β-carotene solution. The plate was then incubated at 45 °C for 120 min. Absorbance measurements were taken at 470 nm at 0

min and after 120 min using a CLARIOstar plate reader (BMG LABTECH, Germany). The bleaching rate of β-carotene and the percentage of antioxidant activity were calculated using the following equations:

$$\text{Bleaching rate} = \text{Ln}\frac{\text{Abs0}}{\text{Abs120}} * \frac{1}{120}$$

$$\text{Antioxidant activity\%} = \left(\frac{\text{BRcontrol} - \text{BRsample}}{\text{BRcontrol}}\right) * 100$$

where *Abs0* is the absorbance value in time 0, *Abs120* is the value of the absorbance at 120 min and *BR* is the bleaching rate.

2.8. Material characterization

2.8.1. Visual appearance and microscopic analyses

The cellulose fibers, after chemical and mechanical modifications, were observed using laser FV 1000-IX81 confocal scanning microscope (CLSM, Olympus, Japan) and Calcofluor White stain. Images were analyzed and processed by using FV10-ASW Version 4.02.03.06 (Olympus Corporation, Tokio, Japan). Furthermore, the surface morphology of the materials and cellulose nanofibril distribution were evaluated using digital macrophotography. Samples were imaged at magnifications of 2× and 20× using an EVOCAM-II macroscope (Vision Engineering, Woking, UK). Image acquisition was performed with ViPlus v1.00.82 software (2018, Vision Engineering), and subsequent image analysis was conducted using Nis Elements BR 3.2 software (Nikon Corporation, Japan). Additionally, light microscopy was used to further elucidate the appearance of the surface of the materials, the organization of the cellulosic fibers, and the porosity of the aerogels and cryogels. Images were acquired using a Nikon Eclipse 90i wide-field microscope (Nikon Corporation, Japan) equipped with a cooled, 5-megapixel digital color camera (DS-5Mc; Nikon Corporation; Japan). The microstructure of the aerogels and cryogels was investigated using SEM. Small samples (approximately 5 mm^2) were sputter-coated with a gold-palladium mixture under vacuum for 3 min. Morphology was examined using a Hitachi S-4800 scanning electron microscope (Hitachi High-Technologies Corporation, Tokyo, Japan) at an accelerating voltage of 10 kV and a working distance of 8–16 mm.

2.8.2. Density and porosity

The density of each aerogel and cryogel sample was determined gravimetrically by measuring its weight and volume. The weight of each sample was measured using an analytical balance (model MS105DU, Mettler-Toledo GmbH, Spain). The dimensions of each sample were measured using a digital caliper (VWR International, USA). Additionally, the specific surface area was determined using the Brunauer-Emmett-Teller method (BET), according to Méndez et al. (2023). The determinations were carried out in triplicate for density and duplicate for BET analysis.

2.8.3. Antioxidant capacity of the cryogels

The antioxidant capacity of the cryogels was evaluated using the β-carotene bleaching method according to Fontes-Candia et al. (2019) with some modifications. In particular, the same conditions and calculations described in Section 2.10 were used, but in this case, the volume was increased. For this purpose, 2.5 mL of the β-carotene solution was placed in Pyrex tubes, and then both the whole antioxidant-impregnated and the control cryogels were immersed. At time 0 and 120 min after incubation at 45 °C, 1 mL of the supernatant was sampled to measure the absorbance at 470 nm in a UV–Vis spectrophotometer (Agilent Technologies, USA). The calculations were performed as described in Section 2.7.

2.8.4. Water vapor sorption capacity

The water vapor sorption capacity of the materials was assessed according to Cabrera-Villamizar, Campano, et al. (2024) using a closed systems to evaluate water uptake until saturation. Aerogel and cryogel samples were pre-treated by heating at 60 °C for 2 h to remove adsorbed moisture, followed by cooling in a desiccator with silica gel for complete drying. The dry weight of each sample was measured using an analytical balance (model MS105DU, Mettler-Toledo GmbH, Spain). Samples were then placed in a desiccator with distilled water to create a 100 % relative humidity environment, monitored by a thermohygrometer. Weights were periodically recorded until water equilibrium (W_e) and saturation were achieved, enabling the determination of the materials' water vapor sorption capacity.

2.8.5. Water sorption capacity

The water sorption capacity was determined by immersing a pre-weighted sample of 1 × 1 cm of the materials. The materials were equilibrated (dried) at 60 °C for 2 h and in a desiccator with silica gel until reaching room temperature to eliminate residual water. Subsequently, their weights were measured using an analytical balance (model MS105DU, Mettler-Toledo GmbH, Spain). Then, the samples were immersed in 15 mL of distilled water at room temperature (22 ± 2 °C), and their mass was determined at predetermined time intervals (0.5, 1, 1.5, 2, and 4 h). The absorbed water over time was calculated based on the difference of the mass on a determinate time point minus the initial dry weight of the material.

2.8.6. Compressibility

Compression tests were performed on the materials using an INSTRON 34TM-5 Dual Column Tabletop Model (Instron Corporation, USA) at a strain rate of 5 mm/min at the temperature of 22 ± 2 °C and relative humidity of 60 ± 5 %. A compression deformation test was conducted with a minimum force of 0.05 N applied to the samples using the parallel plates accessory. The tests were carried out using aerogels and cryogels with determined dimensions (10 × 5 mm) and (14 × 10 mm), respectively. To ensure data accuracy, a minimum of two samples were tested.

2.8.7. Thermogravimetric analysis (TGA)

Thermogravimetric analysis (TGA) was performed using a TGA 550 instrument (TA Instruments, USA). Samples were heated from 30 °C to 850 °C at a heating rate of 20 °C/min under an air atmosphere. Derivative thermogravimetric (DTG) curves were analyzed to identify weight loss events as a function of temperature. The thermal degradation behavior of the samples was determined, and the percentage of ash content was calculated as the residual mass after the completion of the temperature program.

2.8.8. Fourier-transform infrared spectroscopy (FTIR)

FTIR analyses were performed in attenuated total reflectance (ATR) mode using a Thermo Nicolet Nexus (Thermo Fisher Scientific, Waltham, MA, USA) spectrometer (Thermo Fisher Scientific, Waltham, MA, USA). Samples were placed on the ATR crystal for analysis at room temperature (22 ± 2 °C). The spectra were collected with a resolution of 4 cm^{-1} in the wavenumber range of 4000–600 cm^{-1}, co-adding a minimum of 32 scans.

2.9. Challenge test

The feasibility of using cryogels for meat storage was evaluated through an experiment comparing the storage of minced beef for 9 d alone, with a commercial plastic pad, with cryogels and rice-straw-impregnated cryogels. All the treatments were performed in triplicate. Two concentrations of the rice straw were tested, 75 and 187.5 mg/g, and, the addition of the extract was performed in powder before drying. Briefly, 10 g of the obtained homogenized suspensions were poured into 60 mm Petri dishes. The suspensions were then frozen at −80 °C and subsequently freeze-dried. The antioxidant capacity of the resulting cryogels was determined as described in Section 2.8.3. Then, all the

tested materials were placed in Petri plates, and UV sterilized for 30 min.

The fresh beef was ground using a meat grinder to achieve homogeneity, and 12 g of minced beef was placed on top of the materials under aseptic conditions. The plates were sealed with Parafilm to prevent desiccation and microbial contamination. The prepared samples were stored at 4 °C for 9 d. To assess the impact of cryogel storage on meat quality, colorimetric values, malondialdehyde (MDA) concentration, and lipid oxidation were measured in the meat samples. Measurements were obtained both before and after the 9-d storage period.

2.9.1. Colorimetry

Color measurements were taken directly from the meat surface using a target mask (MAV, measurement area 8 mm diameter) attached to a spectrophotometer (CM26dG, Konica Minolta, Japan). The measurements were carried out in triplicate, and each replicate consisted of three subsamples. CIE-L*a*b* coordinates, Lightness (L*), hue (h^*_{ab}), chroma (C^*_{ab}) and the total color differences (ΔE) were obtained from the reflection spectra of the samples using D65 illuminant/10° observer.

2.9.2. Determination of myoglobin, oxymyoglobin and metmyoglobin

Myoglobin content (% Mb), oxymyoglobin (% O_2Mb), and metmyoglobin (% MetMb) were determined according to a modified method described by Carlez et al. (1995). Briefly, 2 g of meat samples were homogenized with 20 mL of 0.04 mol/L phosphate buffer solution (PBS) (pH 6.8) using an Ultra-Turrax homogenizer until homogeneous suspensions were obtained. The homogenates were then kept on ice for 1 h, followed by centrifugation at 4200 rpm for 30 min at 10 °C. The supernatants were filtered through 0.45 μm filters and then they were volume up to 25 mL with PBS. Aliquots of 250 μL were pipetted into a 96-well plate, and absorbance was measured at 525, 545, 565, and 572 nm using a CLARIOstar plate reader (BMG LABTECH, Germany). The following equations were used to calculate the percentages of Mb, O_2Mb, and MetMb:

$$\%Mb = (0.369\,R1 + 1.140\,R2 - 0.941\,R3 + 0.015)*100$$

$$\%O2Mb = (0.882\,R1 - 1.267\,R2 + 0.809\,R3 - 0.361)*100$$

$$\%MetMb = (-2.541\,R1 + 0.777\,R2 + 0.800\,R3 + 1.098)*100$$

where R1, R2 and R3 are respectively the absorbance (A) ratio A572/A525, A565/A525, A545/A525.

2.9.3. Lipid oxidation determination by thiobarbituric acid reactive substances (TBARS)

Lipid oxidation in the samples was evaluated before and after the 9-d storage period using the TBARS assay as described by Fontes-Candia et al. (2019) with minor modifications. Briefly, 5 g of meat was homogenized with 15 mL of distilled water using an Ultra-Turrax homogenizer. The homogenate was then transferred to a 1 L volumetric flask along with 32.5 mL of distilled water. The pH was adjusted to 1.5 using HCl. Subsequently, 0.5 mL of 10 % (w/v) EDTA, 0.5 mL of 10 % (w/v) ethanolic propyl gallate, two drops of antifoam silicone, and five glass pearls were added to the flask. The flask was connected to a Soxhlet apparatus, and the mixture was refluxed until 50 mL of distillate was collected.

For TBARS determination, 5 mL of the distillate was combined with 5 mL of 0.02 M TBA solution in 90 % acetic acid within a screw-capped test tube and incubated in a boiling water bath for 35 min. A control sample containing 5 mL of distilled water and 5 mL of TBA reagent was incubated alongside the samples. After cooling to room temperature, the absorbance of all samples and the control was measured at 535 nm using a spectrophotometer. TBARS concentration was calculated by multiplying the absorbance values by a factor of 7.8 and expressed as mg malondialdehyde (MDA)/kg meat.

2.10. Statistical analysis

Statistical analyses were performed to assess significant differences between groups. Analysis of variance (ANOVA) was employed to test the null hypothesis of no difference between treatment groups. Following a significant ANOVA result ($p < 0.05$), Tukey's Honestly Significant Difference (HSD) post-hoc test was conducted to identify which specific groups differed from each other.

3. Results and discussion

3.1. Cellulose extraction

Compositional analysis was first performed on the raw biomass (*C. sativa* stems) and cellulosic fraction and the results are summarized in Table 1. The cellulosic extraction yield was 65.89 ± 7.33 %, which is similar to the values reported in the literature for cellulosic hemp materials (Barbash et al., 2016). As expected, the cellulosic fraction was enriched after the extraction process, cellulose being predominant and reaching values of 79.47 %. Although the lignin and the hemicellulose contents were significantly reduced in the cellulose-rich extract, amounts of 3.50 and 14.02 %, respectively, were still present, indicating the presence of recalcitrant lignin.

The cellulosic extract was further characterized by FTIR and TGA. Typical lignocellulosic bond vibrational bands were observed. For instance, the FTIR analysis shown in Fig. S1A revealed a broad peak at 3600–3000 cm^{-1}, characteristic of O—H stretching, attributed to hydrogen bonding between hydroxyl groups in cellulose and hemicellulose (Geminiani et al., 2022). Additionally, peaks around 1730 and 1500 cm^{-1} indicated the presence of carbonyl and aromatic structures, respectively. These functionalities are associated with ester linkages in hemicellulose and lignin (Le Troedec et al., 2008); however, their low intensity suggests a low lignin content, as expected. Finally, the peak at 1030 cm^{-1}, characteristic of stretching vibrations, was assigned to the pyranose ring skeletal vibration of cellulose (Mhlongo et al., 2022).

Thermogravimetric analysis, as shown in Fig. S1B, revealed a three-step degradation profile. An initial weight loss of 7 % occurred between 60 and 100 °C, attributed to water evaporation. Subsequently, an exothermic peak at 280 °C corresponded to cellulose decomposition, accounting for 86 % of the total weight loss. The final degradation stage, between 300 and 400 °C, was indicative of lignin decomposition, consistent with previous studies on hemp lignocellulosic extracts (Rachini et al., 2009).

3.2. Aerogels and cryogels development

Cellulosic aerogels and cryogels, despite their initially robust porous structure, exhibit instability when submerged in water. This instability manifests as dispersion or resuspension within the aqueous medium. This behavior is attributed to cellulose's inherent hydrophilicity, the material's highly porous structure facilitating rapid water penetration, and the disruption of weak intermolecular forces, such as hydrogen bonds, by water molecules. Previous research has addressed this issue by applying polymeric coatings to enhance the hydrophobicity of cellulosic

Table 1
Compositional analysis of the raw material (*C. sativa* stems) and of the lignocellulosic extract.

Component (%)	*C. sativa* stems	Cellulosic fraction
Cellulose	41.21 ± 1.89	79.47 ± 0.70
Hemicellulose	21.43 ± 3.01	14.02 ± 0.75
Lignin	22.06 ± 2.96	3.50 ± 0.16
Protein	8.01 ± 0.05	*
Lipid	1.34 ± 0.01	*
Ash	2.96 ± 0.03	3.00 ± 0.06

* Undetermined values.

materials (Benito-González et al., 2020), thereby preventing water absorption and preserving structural integrity in aqueous environments. However, to simplify end-of-life management and disposal, a monomaterial approach is preferred. Consequently, chemical modification emerges as a necessary strategy to prevent the dispersion or disintegration of cellulosic aerogels and cryogels. To address this, a two-step process was implemented: TEMPO-oxidation for stabilization and high-pressure homogenization for defibrillation. This approach aimed to create aerogels and cryogels with enhanced stability and well-defined porous structures. TEMPO-mediated oxidation (TEMPO-NaBr-NaClO) is known to generate TEMPO-oxidized cellulose nanofibrils, which, when transformed into aerogels and cryogels, exhibit unique thermal conductivities, filtration behaviors and mechanical properties (Puangsin et al., 2017). Additionally, TEMPO-oxidized cellulose coupled with high-pressure homogenization, in contrast to the unoxidized counterparts, has proven to improve mechanical properties, increase the surface area, allowed better dispersion and stability of the nanofibrils suspension, produces a wide range of porous materials, enhance water sorption capacity (Darpentigny et al., 2020; Lee et al., 2009; Pirozzi et al., 2023).

The effectiveness of the oxidation treatment was evaluated by quantifying the carboxyl group content in the treated cellulose compared to the untreated material. The concentration significantly increased from 0.11 mmol/g to 0.69 mmol/g after oxidation. Additionally, confocal microscopy and transmission electron microscopy (Fig. S2) confirmed the successful isolation of cellulose fibers. Interestingly, hemp cellulose only required three high-pressure homogenization passes to achieve the desired level of fibrillation, compared to eight passes required for rice straw cellulose (Cabrera-Villamizar, Campano, et al., 2024). This highlights the ease of oxidation and defibrillation of hemp stem cellulose compared to other biomass sources, potentially reducing processing steps, energy consumption and production time.

Using established drying methods, the stabilized cellulose suspension was successfully used to produce both aerogels and cryogels. Aerogel production involved a solvent exchange process, where water was replaced with ethanol to facilitate subsequent dissolution and removal via SC-CO_2. To enable this exchange, the oxidized cellulose suspension underwent cross-linking with citric acid, inducing a sol-gel transition. Citric acid is a well-known crosslinking agent for various cellulose derivative systems (Demitri et al., 2008). As previously mentioned, the crosslinking concentration was 0.5 M. This concentration could produce stable hydrogels without brittleness. As previously reported, if the concentration of citric acid used was too low, the brittle hydrogel might be susceptible to shape-changing during the demolding phase (Nasution et al., 2022). Additionally, citric acid has proven to be a non-toxic, non-carcinogenic, more sustainable alternative to traditional cross-linkers, enhancing the hydrogel's performance and biodegradability. The resulting stable hydrogels were then manipulated for solvent exchange, followed by SC-CO_2 drying of the obtained alcogels (Fig. S3).

As shown in Fig. 1A, aerogels and cryogels exhibited distinct macro- and microscopic features. Aerogels displayed significantly smoother surfaces compared to the irregular surfaces observed in cryogels. Cryogels also presented sheet-like structures and possessed larger pores than aerogels. This aligns with previous reports (Buchtová & Budtova, 2016), demonstrating that freeze-drying leads to a sheet-like cellulose network with large and interconnected pores (several micrometers) due to ice crystal growth during water freezing. Consequently, the porosity of the aerogels was expectedly lower than that of the cryogels, as it will be shown below.

3.3. Aerogels and cryogels characterization

BET analysis confirmed the anticipated differences in porosity between cryogels and aerogels. Due to the large pores within their structure, cryogels could not retain the nitrogen gas required for surface area measurement. Freeze-drying, a step in cryogel preparation, replicates the sublimated ice crystals within the hydrogel network, resulting in a highly porous structure with pores ranging from microns to hundreds of microns (Buchtová et al., 2019). This ice crystal formation can compress the cellulose fibrils, potentially sacrificing some nanostructure in the pore walls. Conversely, the aerogels displayed a typical mesoporous structure with a BET surface area of 295.13 m^2/g, an average pore diameter of 7.17 nm, and an average pore width of 14.02 nm (BJH adsorption). Notably, the obtained pore width is significantly smaller compared to other cellulose aerogels. For instance, Darpentigny et al. (2020) reported an average pore size of 24.7 ± 10.4 μm using TEMPO-oxidized cellulose nanofibrils. This difference suggests that hemp cellulose exhibits unique properties after oxidation, contrasting with wood pulp cellulose used in aerogel development. Scanning electron

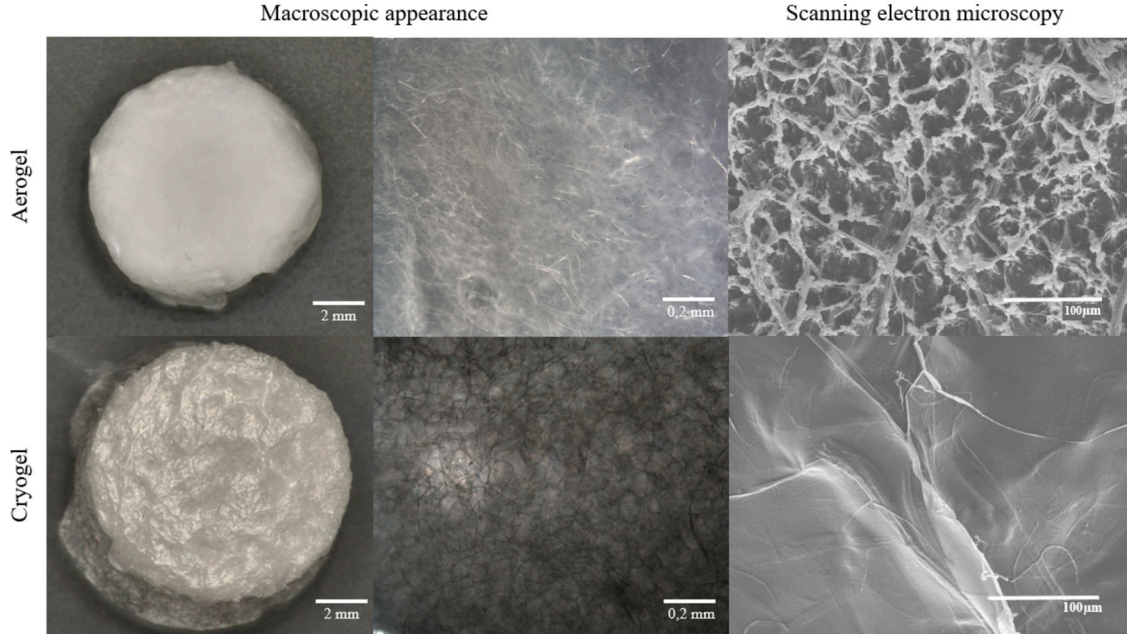

Fig. 1. Macroscopic and microscopic characterization of aerogels and cryogels. Macroscopic appearance under two different magnifications captured using macrophotography equipment. Microscopic structure as visualized by scanning electron microscopy (SEM).

microscopy (SEM) images corroborated these observations regarding the porosity of the materials (see Fig. 1). Additionally, as shown in Fig. S4, the pore distribution area analyzed using SEM images showed a range of sizes below 900 μm^2 for cryogels and below 70 μm^2 for aerogels. Density analysis revealed no statistically significant differences between the aerogels ($5.0 \times 10^{-4} \pm 7.0 \times 10^{-5}$ g/cm^3) and cryogels ($4.7 \times 10^{-4} \pm 3.0 \times 10^{-5}$ g/cm^3). Although aerogels exhibited slightly higher density, this variation was negligible.

Following characterization, the compressive strength of the materials was evaluated (Fig. 2A). Aerogels displayed significantly higher compressive strength (40.01 kPa at 50 % compressive deformation) compared to cryogels (19.10 kPa). This difference can be attributed to the denser structure and internal pore distribution of aerogels. Interestingly, both aerogels and cryogels exhibited 2–3 times greater resistance to compression compared to carbon aerogels derived from TEMPO-oxidized cellulose nanofibrils (Lai et al., 2021). This superior performance can be linked to the inherent flexibility and compression resistance of cellulose nanofibril aerogels (Zhu et al., 2022). Additionally, as previously reported by Zheng et al. (2020) one of the technical strategies to improve starch-based aerogel is the use of lignocellulose nanofibrils to increase the mechanical strength, making the developed materials stronger to compression in contrast to starch-based aerogels.

A crucial factor for industrial applications is control over material size and shrinkage during production and use. The diameter and shrinkage of the materials were monitored throughout processing (Table 2). Aerogels exhibited minimal dimensional changes in diameter after gelation. However, a significant reduction occurred following SC-CO_2 drying and decreased further upon exposure to water vapor sorption tests. The aerogels might present this shrinkage behavior due to capillary condensation and hydrogen bonding. Thus, water vapor condenses in the nanopores, creating surface tension forces that pull the pore walls together (Paulauskiene et al., 2024). In addition, the hydrophilic cellulose nanofibrils formed new hydrogen bonds with the water molecules, leading to structural rearrangement and collapse of the porous network (Zaman et al., 2020b). Furthermore, previous studies reported that the pressures above 13 MPa during SC-CO2 drying could minimize shrinkage in cellulose nanofibrils (Zhu et al., 2022); however, in the present study the used pressure was 12.1 MPa which may lead to the unstable structure. In consequence, the shrinkage upon water exposure limits the potential application of aerogels as meat-absorbent pads.

In contrast, cryogels displayed minimal dimensional changes across

Table 2
Diameter of the aerogels and cryogels in their suspension, gelled, dried, and after water vapor sorption test states.[a]

Material state	Aerogels diameter (mm)	Cryogels diameter (mm)
Suspension	15.00 ± 0.00[a]	15.00 ± 0.00[a]
Gelified	14.24 ± 0.45[a]	15.00 ± 0.45[a]
Dried	10.32 ± 0.52[b]	14.14 ± 0.19[a]
After water vapor sorption	8.00 ± 1.04[c]	13.79 ± 0.20[a]

[a] Different letters represented significant differences.

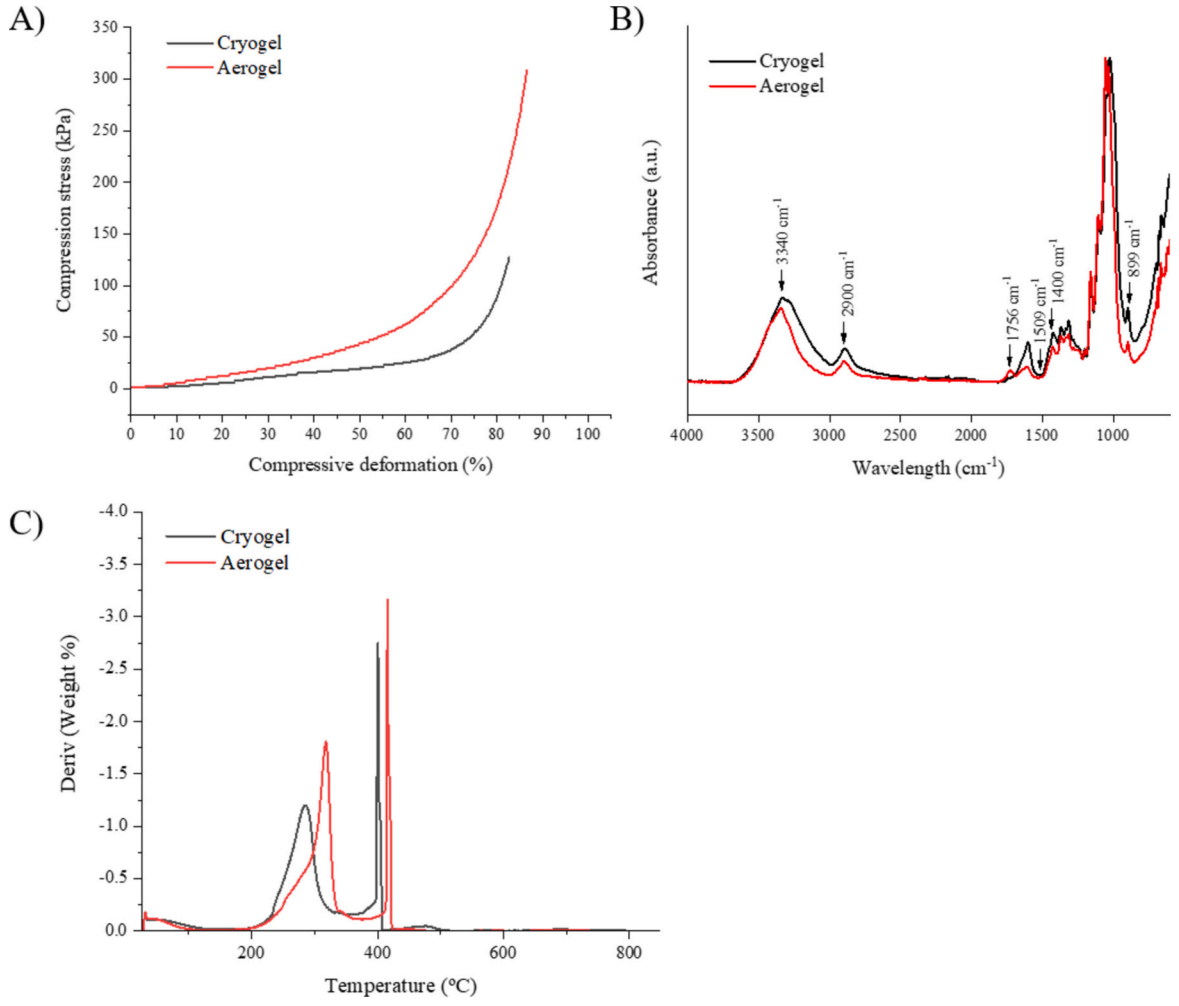

Fig. 2. A) Compressive stress-strain curves of aerogels and cryogels. B) FTIR spectra of the aerogel and cryogel samples. D) Derivative thermogravimetric (DTG) curve depicting the rate of weight loss versus temperature.

all processing stages, demonstrating remarkable stability throughout processing and potential use. The stability of this material might be explained because the larger pores are less susceptible to capillary condensation effects and after the freeze-drying process, stronger interfibrillar bonds make the structure more resistant to rearrangement (Zhang et al., 2015). Therefore, cryogels may be better suited for meat-absorbent pads application.

Additionally, another important factor during the development of absorbent pads is undoubtedly their capacity to sorb and retain water. Therefore, the water vapor sorption capacity was used to evaluate the capacity of saturation and water sorption water from the closed 100 % RH environment. The aerogels retained 1.86 ± 0.10 mL/g, and the cryogels retained 2.20 ± 0.004 mL/g after equilibrium (W_e). The results showed significant differences and illustrated that cryogels were capable of sorbing more water than aerogels, thus, making them more suitable for sorption applications. Additionally, other food cellulosic aerogels showed that water vapor sorption capacity was significantly lower than the one reported in the present study due to the use of crystalline cellulose (Ciuffarin et al., 2023). Therefore, the use of cellulose fibers containing both crystalline and amorphous regions increases the water vapor sorption capacity of the materials.

The FTIR and TGA analyses of the materials corresponded with the compositional analysis of the hemp cellulose, showing the typical lignocellulosic material behavior. Particularly, FTIR analysis revealed subtle variations in the chemical bonding profile of the aerogels and cryogels (Fig. 2B). In the 3700–3000 cm^{-1} region, both samples exhibited a broad peak assigned to the intramolecular hydrogen bonding within cellulose (Cichosz & Masek, 2020). Additionally, a peak at 2900 cm^{-1}, corresponding to C—H stretching in aromatic methyl groups, was identified in both materials, indicating the presence of cellulose and hemicellulose. The peak typically observed in hemp fibers at 1756 cm^{-1}, indicative of hemicellulose content, was minimal due to the reduction following extraction and processing (Vârban et al., 2021). Furthermore, the absence of a peak at 1509–1508 cm^{-1} suggested low lignin content in both samples. Notably, this peak was even lower in the aerogels, potentially due to lignin extraction during SC-CO_2 drying, as previously reported by Yang et al. (2018) and Šutka et al. (2013). Interestingly, the 1428–1400 cm^{-1} region displayed distinct peaks characteristic of crystalline cellulose. Similarly, peaks at 899–894 cm^{-1}, as reported by Vârban et al. (2021) confirmed the presence of glycosidic bonds and the amorphous cellulose region in both samples. These peaks were mainly presented in cryogels, which would allow the retention of more water during the water vapor sorption test. Additionally, thermogravimetric analysis revealed a three-step degradation process for aerogels and cryogels. As shown in Fig. 2C, the aerogel exhibited superior thermal stability. The degradation peaks for the aerogel occurred at 57.7 °C, 317.73 °C, and 416.25 °C. In contrast, the cryogels exhibited lower degradation temperatures at 56.78 °C, 285.77 °C, and 400.73 °C. These results are comparable to the findings reported by Mijas et al. (2021) for hemp fiber degradation. Briefly, the first peak observed between room temperature and 100 °C corresponds to the removal of moisture and volatile compounds. The second degradation step, occurring around 270–290 °C, is attributed to the decomposition of low-to-medium molecular weight hemicelluloses and lignin. Finally, the degradation peak at 390–400 °C is associated with the decomposition of cellulose and medium-to-high molecular weight lignin (Mijas et al., 2021; Rachini et al., 2009). TGA revealed greater thermal stability for aerogels compared to cryogels. This observation likely correlates with a reduction in lignin-like compounds and their derivatives within the aerogels. SC-CO_2 drying potentially removes these moieties due to their solubility in both CO_2 and ethanol. Consequently, the drying process removes these thermally labile components from the aerogels, contributing to their enhanced thermal stability.

Among the investigated materials, cryogels displayed the most favorable characteristics for the replacement of traditional plastic absorbent pads used in food packaging. They exhibited minimal dimensional changes and preserved structural integrity throughout processing and subsequent water vapor sorption assays. Notably, cryogels demonstrated superior liquid uptake compared to aerogels. These findings suggest consistent water sorption capacity and appropriate structural stability in cryogels. Owing to these advantageous properties, cryogels were chosen for further evaluation by impregnation with a rice straw extract.

3.4. Bioactive cryogels

To investigate potential structural differences affecting material functionality, the cryogels were characterized following the incorporation of rice straw extract and freeze-drying. This characterization included macro and microscopic analyses, water vapor sorption capacity, water sorption by immersion and desorption capacity, evaluation of the antioxidant capacity, compressibility, TGA and FTIR.

The macroscopic characterization revealed concentration-dependent changes in the coloration of the materials following extract addition, as shown in Fig. 3A. All the treatments displayed homogeneous surface morphology after freeze-drying. The microscopic analysis demonstrated that the pore structure and fiber distribution slightly differed from the impregnated cryogels in contrast to the pristine cryogels. Correspondingly, SEM analysis confirmed that the incorporation of the extract at 187.5 mg/g did not affect the microstructure of the material (Fig. 3B). Notably, the consistent color change across the entire material suggested thorough impregnation with minimal extract aggregation on the fiber surface. These findings indicate successful extract incorporation prior to freeze-drying, with minimal impact on the macro and microscopic morphology of the developed materials. In addition, the visualization of the surface without aggregates might suggest that the incorporation prior to freeze drying did not require any crosslinking agent, as required in previous studies where cellulose and lignin were compatibilized by Fe^{3+} (Sanchez et al., 2023). The antioxidant activity determined by β-carotene bleaching of 2 mg/mL of the rice straw extract was determined to be 47 ± 2.5 %. Correspondingly, Ghasemzadeh et al. (2015) reported similar antioxidant values (47.23 %) after ethanol-water extractions in rice bran. Additionally, the rice straw extract used in the present study was previously characterized by Cabrera-Villamizar, Ebrahimi, et al. (2024) where the antioxidant capacity was 77.53 mg Trolox equivalents (TE)/g and the polyphenol content was 69.20 Equivalent mg Gallic acid/g after the alkaline extraction.

Subsequently, the preservation of the functionality of the rice straw extract within the material was evaluated. The results, shown in Table 3, demonstrated that, at both tested concentrations, 75 mg/g and 187.5 mg/g, the materials showed a high antioxidant activity. The antioxidant properties were attributed to the presence of several previously reported bioactive compounds such as gallic acid, caffeic acid, pyrogallol, flavonoids, phenolic compounds (p-coumaric acid and protocatechuic acid) (Menzel et al., 2020). Particularly, after alkaline extractions from rice straw the main components founded where ferulic acid, p-coumaric acid, vanillic acid, syringaldehyde, p-hydroxybenzaldehyde and vanillin (Li et al., 2015). Similarly, Wu, Wu, et al. (2023) have demonstrated that the grafting of p-coumaric acid with cellulose nanocrystals keep the antioxidant activity after chemical interaction. Furthermore, a positive correlation was observed between the incorporated antioxidant amount and the measured activity, indicating a dose-dependent effect. Conversely, the pristine cryogels (without extracts) did not exhibit antioxidant activity. Furthermore, when comparing to other cellulosic cryogels impregnated with antioxidant extracts (36.8–57.3 %) (Fontes-Candia et al., 2019), the developed materials showed higher antioxidant activity during the β-carotene bleaching assays.

The cryogels with and without the rice straw extract retained the structural integrity after being immersed in water, as shown in Fig. 3C. The materials showed a stable structure despite their hydrophilic intrinsic character and the incorporation of the extract that could interfere with the formed hydrogen bonds between the cellulosic fibers.

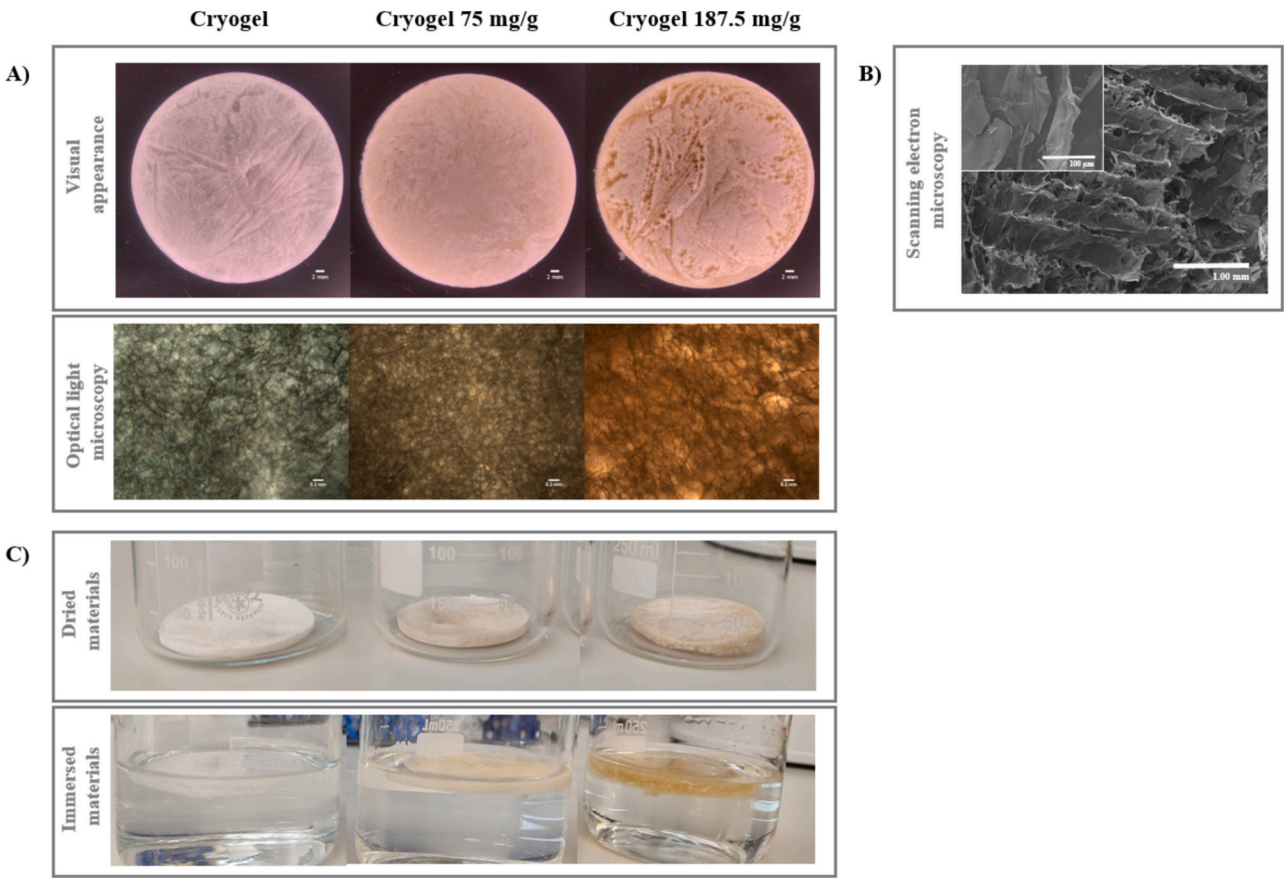

Fig. 3. A) Macroscopic and optical microscopy images of the cryogels before and after impregnation. B) Scanning Electron Microscopy (SEM) images for impregnated material 187.5 mg/g. C) Evaluation of material integrity after immersion in distilled water for 2 h at 22 °C.

Table 3
Antioxidant activity of cryogels containing rice straw extract evaluated by β-carotene bleaching method.[b]

Treatment	Antioxidant activity %
Cryogel	0.01 ± 0.25[a]
Cryogel 75 mg/g	63.89 ± 5.38[b]
Cryogel 187.5 mg/g	78.96 ± 1.84[c]
BHT	98.03 ± 0.41[d]

[b] Different letters represented significant differences.

This points out that the incorporation of the rice straw extract did not cause any alteration in the integrity of the material. An evaluation of the compressibility of the materials revealed that impregnated materials exhibited superior mechanical properties compared to the pristine cryogel. As illustrated in Fig. S5, at 60 % compressive deformation, the cryogels and impregnated materials displayed stress resistances of 25.46 kPa and 44.56 kPa, respectively. Similarly, preliminary studies have demonstrated that the incorporation of lignin derivatives not only enhances the mechanical properties but also contributes to the stability of cellulose aerogels in an aqueous medium (Wang et al., 2023).

Additionally, the incorporation of the rice straw reduced the water vapor sorption capacity (WVSC) to 1.08 ± 0.10 mL/g (1.12 mL/g was reduced). Correspondingly, the absorption and desorption capacity of the cryogels evaluated by immersion showed a similar tendency. Cryogels exhibited superior water sorption capacity compared to the commercial pad, as shown in Fig. 4A. Punctually, at their equilibrium, they can absorb up to 140.71 ± 4.87 mL of water per gram of cryogel, which is 4.8 times greater than the commercial pad's capacity (29.36 ± 0.30 mL/g). Notably, no significant differences in sorption capacity were observed between the pristine cryogel (140.71 ± 4.87 mL/g) and the one impregnated with 75 mg/g of the extract (149.52 ± 4.41 mL/g). However, increasing the antioxidant concentration to 187.5 mg/g resulted in a decrease in sorption capacity (134.66 ± 0.20 mL/g). This can be attributed to the presence of hydrophobic lignin derivatives within the rice straw extract, which have hydrophobic properties, thus mitigating water sorption in the material. This finding is consistent with previous information reported by Mariana et al. (2021), who showed that once lignin was added to other biopolymers, they became more hydrophobic and the materials presented lower water sorption than the biopolymers without any reinforcement in a high-humidity environment. Additionally, the hemp materials showed a slower saturation rate than commercial pads but showed greater sorption capacity. The cryogels exhibited desorption capacity, releasing 95 % of the retained liquid within the first 0.5 h, as shown in Fig. 4B. Conversely, the commercial pad retained moisture and did not achieve complete desorption. This difference arises from the multilayer structure of the commercial pad. It possesses a porous hydrophobic surface, facilitating sorption through the pores. However, the remaining non-porous surface area traps the liquid within the material. Future studies could investigate incorporating a similar protective system onto the cryogels to delay their desorption capacity. This system could involve a biopolymer hydrophobic layer that regulates the sorption rate using the same mechanism, such as the one proposed by Benito-González et al. (2020) where cellulosic cryogels were hydrophobized with poly (lactic acid) making them suitable for water and oil sorption.

Finally, as shown in Fig. 4C, the thermogravimetric analysis results showed a three-step degradation process. However, the incorporation of the extract shifts the temperature of the second degradation peak to lower temperatures, indicating that the incorporation of the extract slightly decreased the thermal stability of the material. The

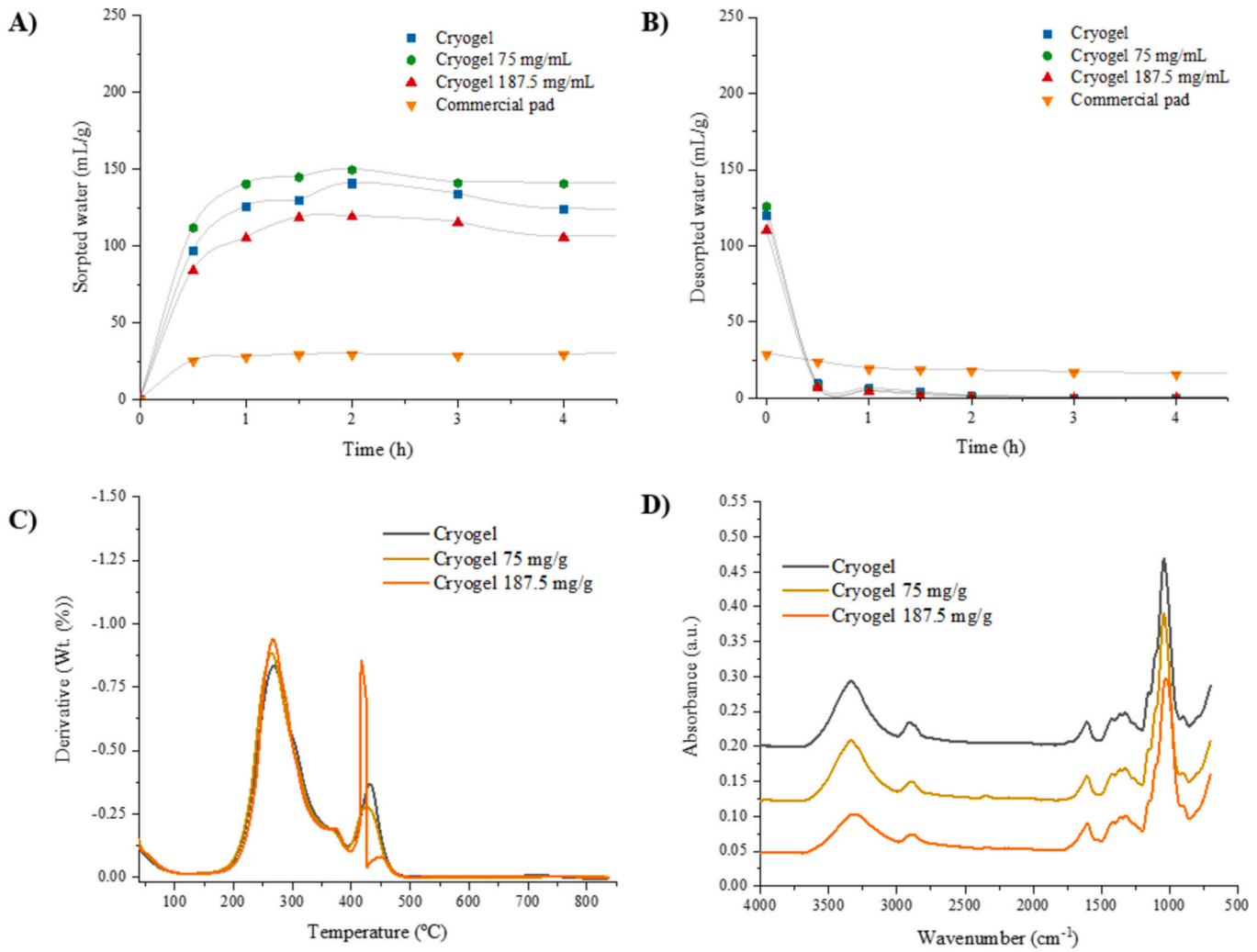

Fig. 4. A) Water sorption and desorption B) isotherms of the cryogels. C) Derivative thermogravimetric curve (DTGA) of cryogels before and after impregnation. D) FTIR spectra of the cryogels and impregnated cryogels.

displacement was concentration-dependent, thus lower for 75 mg/g and higher for 187.5 mg/g treatments. Consequently, the extract's incorporation slightly affected the impregnated cryogel's thermal profile. Liu et al. (2024), have reported the same effect where the incorporation of bioactive compounds such as chitosan reduced the thermal stability of the CNF aerogels. On the other hand, as shown in Fig. 4D, FTIR analysis revealed no changes in the types of chemical bonds present, indicating that impregnation occurred without altering the original bonding structure of the cryogel.

3.5. Challenge test

Following the characterization and functionalization with rice straw extract, the efficacy of the materials as food absorbing pads in minced beef packaging was evaluated during a challenge test. Cryogels, impregnated cryogels and a commercial plastic multilayer pad were compared in a setup shown in Fig. 5A. After storage under refrigerated conditions for 9 d, color change, myoglobin content and the effect of the various pads on lipid oxidation were evaluated.

As shown in Table 4, colorimetric analysis revealed significant color differences between the meat at the initial time and after storage, as anticipated. Specifically, the lightness (L*) parameter showed greater changes in the pristine cryogel samples. Whereas, the commercial pad and the impregnated cryogel (187.5 mg/g) showed smaller lightness changes. Regarding the chroma (C^*_{ab}) parameter, samples with the commercial pads and cryogels exhibit slight darkening compared to the control without pads. Notably, regarding the hue (h^*_{ab}) parameter cryogels (with and without extract) displayed lower opaque values than the control without pad and commercial pad. Finally, with respect to the total color change (ΔE), as shown in Table 2 and Fig. 5B, the use of the cryogel impregnated with 187.5 mg/g resulted in a color change even smaller than that of meat alone and meat stored with the commercial pad. Positively, the incorporation of the bioactive extract showed a lower color change, allowing better preservation of the minced beef color.

Corroborating the colorimetric results, the proportion of myoglobin redox forms was determined to understand their relationship to the observed color changes. It is known that meat color stability depends on maintaining the oxygenated form (oxymyoglobin), which contributes to a bright red color. Thus, the oxidation of myoglobin to ferric (Fe^{3+}) metmyoglobin is a well-established phenomenon causing the undesirable meat color (Carlez et al., 1995). The analyses demonstrated that the myoglobin content did not significantly differ between pre- and post-stored samples, as shown in Fig. 5C. Conversely, oxymyoglobin levels decreased in all samples after storage. However, cryogel containing 187.5 mg/g of the extract displayed a slightly higher oxymyoglobin content after storage, indicating improved redness retention in the meat. This finding aligns with the colorimetric data (total color change ΔE), suggesting that the rice straw extract enhances the preservation of the red color during meat storage. In contrast, metmyoglobin content

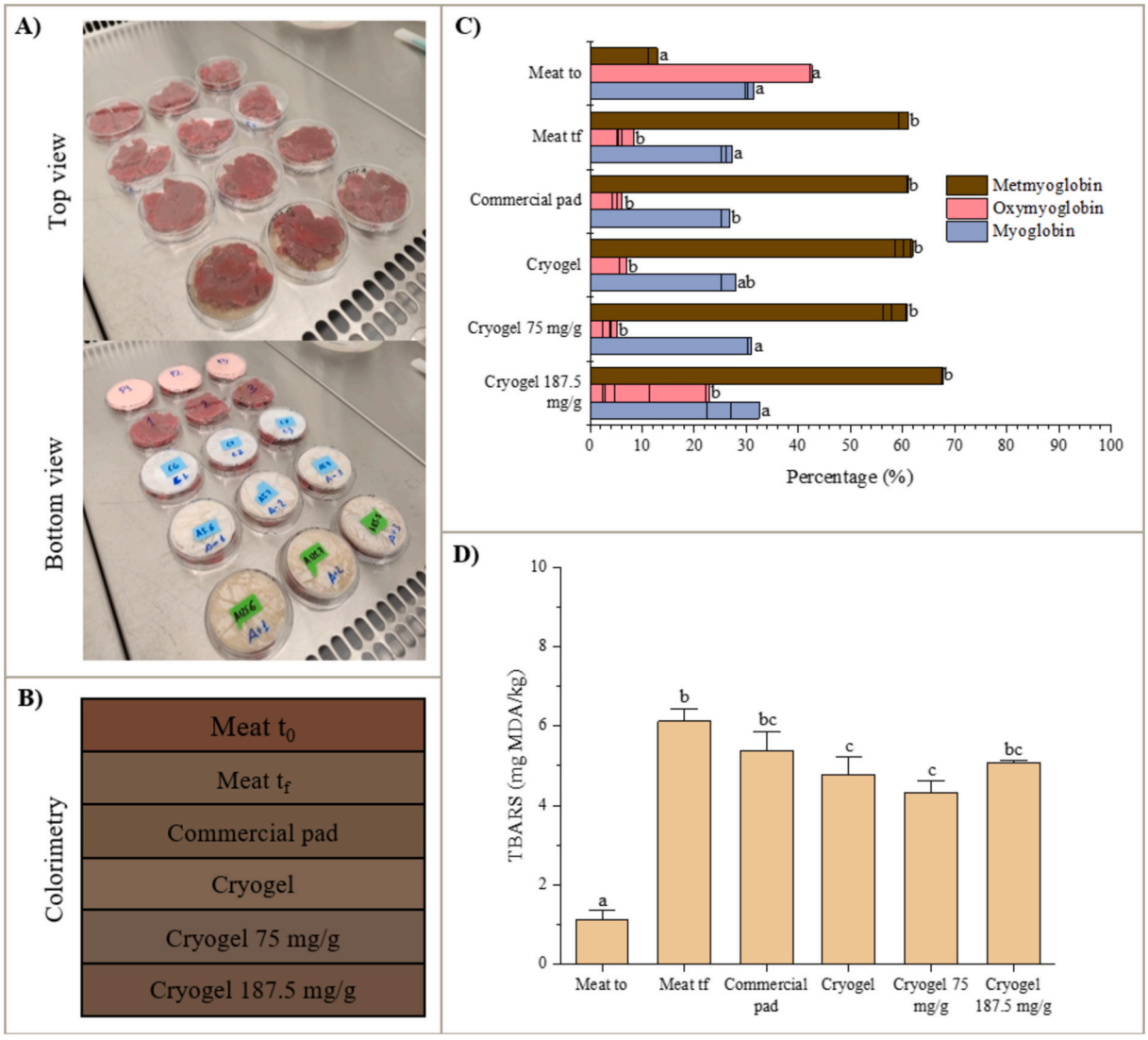

Fig. 5. Beef proof-of-concept. A) Top and bottom views: Commercial pad, minced beef alone, cryogels, and impregnated cryogels. B) Color analysis: Reproduced color using L*, C*, and h* parameters for meat before storage (t_0) and after storage (t_f), including meat alone, the commercial pad, cryogel, and impregnated cryogels. C) Myoglobin redox forms: Percentage of Myoglobin (Mb), Oxymyoglobin (OxyMb), and Metmyoglobin (MetMb). D) Lipid oxidation: TBA reacting substances (TBARS).

Table 4
Colorimetric parameters before (day 0) and after (day 9) the packaging period. Different letters denote significant differences between treatments.

Time	Treatment	ΔE	Lightness (L*)	Chroma (C*)	Hue (h°)
Day 0	Meat	0.00 ± 0.00^{a}	35.17 ± 0.51^{a}	24.91 ± 1.05^{a}	50.92 ± 0.61^{a}
Day 9	Meat	11.75 ± 0.25^{c}	41.7 ± 0.40^{c}	17.07 ± 0.15^{b}	67.12 ± 0.28^{e}
	Commercial pad	11.15 ± 0.29^{c}	39.77 ± 1.12^{b}	$16.74 \pm 0.32^{b,c}$	67.73 ± 0.10^{e}
	Cryogel	13.72 ± 1.39^{d}	44.08 ± 0.83^{d}	15.62 ± 1.43^{c}	64.57 ± 0.16^{d}
	Cryogel 75 mg/g	14.47 ± 0.01^{d}	$42.13 \pm 0.46^{c,d}$	12.43 ± 0.28^{d}	58.09 ± 0.41^{b}
	Cryogel 187.5 mg/g	9.19 ± 0.19^{b}	37.96 ± 0.22^{b}	$16.79 \pm 0.36^{b,c}$	60.03 ± 1.00^{c}

Different letters denote significant differences between treatments.

increased in all treatments after storage, as expected, reaching up to 70 % compared to <20 % at the initial time. Additionally, the added extract, rich in polyphenols, might influence the reduction of Fe^{3+} to Fe^{2+}, temporarily maintaining or restoring the red color (Maurya & Devasagayam, 2010).

On the other hand, as expected after a 9-d storage period, the lipids presented in minced beef were oxidized, as shown in Fig. 5D. The storage with the commercial pad did not show significant differences with respect to the meat itself. On the other hand, the cryogel showed differences in reducing the concentration of MDA detected. This might indicate that the type of material helps to reduce oxidation during storage. Similarly, the 75 mg/g impregnated cryogel showed a reduction of the oxidized lipids concerning the meat alone, indicating that the antioxidant effect of the active pad was effective. However, the 187.5 mg/g impregnated cryogel showed no antioxidant activity and behaved similarly to the meat alone. This phenomenon can be attributed to the concentration-dependent antioxidant/pro-oxidant behavior of polyphenols, as observed in rice straw compounds (Table S1). For example,

ferulic acid can act as ferric reducing agent in the Fenton reaction under certain conditions (Maurya & Devasagayam, 2010). This activity is linked to its ability to interact with iron in the meat. The reduced Fe^{2+} can then react with oxygen or other oxidizing agents, regenerating Fe^{3+}. This cycle could accelerate oxidation processes in the meat.

Therefore, the cryogels and the 75 mg/g impregnated materials effectively reduced lipid oxidation. Additionally, cryogels can be an alternative to commercial pads as they behave similarly. Nevertheless, the concentration of the extract should be added carefully to avoid a pro-oxidation behavior. Thus, incorporating the bioactive extract might help with color preservation but slightly enhance lipid oxidation. For instance, Domínguez et al. (2019) demonstrated that stable or low-reactive products are formed from radicals by an atom or group transfer process during lipid oxidation. However, termination reactions are inefficient and may lead to new reactive compounds. Therefore, some of the molecules acting as antioxidants might react and produce reactive free radicals that enhance lipid oxidation during storage.

4. Conclusions

This study explored the potential of hemp cellulose-based aerogels and cryogels for sustainable food packaging applications. The research successfully extracted cellulose from hemp and developed both aerogels (using SC-CO_2 drying) and cryogels (via freeze-drying). While both materials demonstrated good potential, cryogels emerged as the preferred choice due to lower shrinkage, superior water sorption capacity and suitability for impregnation with bioactive compounds. Incorporating rice straw extract, a natural antioxidant source, further enhanced the functionality of cryogels. The extract improved the color preservation of minced beef during storage, likely due to its antioxidant properties and the ability to maintain oxymyoglobin content. Cryogels and 75 mg/g impregnated cryogels exhibited a moderate protective effect against lipid oxidation. However, the impregnated cryogels with a higher concentration (187.5 mg/g) induced pro-oxidant reactions. This work demonstrates the promising potential of hemp cellulose cryogels loaded with natural antioxidants for active food packaging. These bio-based materials offer excellent moisture management properties, improved color preservation and the potential for extending shelf life through their antioxidant activity. Future research should optimize the extract concentration to best balance color preservation and lipid oxidation control. This approach can contribute significantly to developing sustainable and functional biopolymeric packaging solutions for the food industry.

CRediT authorship contribution statement

Laura Cabrera-Villamizar: Methodology, Investigation, Data curation. **Jéssica Fernanda Pereira:** Methodology, Investigation. **María Castanedo:** Methodology. **Amparo López-Rubio:** Writing – review & editing, Visualization, Supervision, Methodology, Investigation, Funding acquisition, Conceptualization. **María José Fabra:** Writing – review & editing, Visualization, Supervision, Project administration, Methodology, Funding acquisition, Conceptualization.

Declaration of competing interest

The authors declare that there are no conflicts of interest.

Acknowledgement

Grants PID2020-112766RB-C22, PID2023-146557OB-C22 and PCI2024-153409 funded by MICIU/AEI/10.13039/501100011033 and, by ERDF A way of making Europe. Laura Cabrera-Villamizar acknowledges financial support from the Generalitat Valenciana for the award of a Santiago Grisolía grant (GRISOLIA/2021/050). The Accreditation as Center of Excellence Severo Ochoa CEX2021-001189-S funded by MCIU/AEI/10.13039/501100011033 is also fully acknowledged.

Appendix A. Supplementary data

Supplementary data to this article can be found online at https://doi.org/10.1016/j.carbpol.2024.122887.

Data availability

Data will be made available on request.

References

Ahmed, A. F., Islam, M. Z., Mahmud, M. S., Sarker, M. E., & Islam, M. R. (2022). Hemp as a potential raw material toward a sustainable world: A review. *Heliyon, 8*(1). https://doi.org/10.1016/j.heliyon.2022.e08753

Barbash, V., Karakutsa, M., Trembus, I., & Yaschenko, O. (2016). Development the technology of obtaining microcrystalline cellulose from the hemp fibers. *Technology Organic and Inorganic Substances, 3*(6), 51–56. https://doi.org/10.15587/1729-4061.2016.71275

Beluns, S., Gaidukovs, S., Platnieks, O., Gaidukova, G., Mierina, I., Grase, L., … Thakur, V. K. (2021). From wood and hemp biomass wastes to sustainable nanocellulose foams. *Industrial Crops and Products, 170*, Article 113780. https://doi.org/10.1016/j.indcrop.2021.113780

Benito-González, I., López-Rubio, A., Galarza-Jiménez, P., & Martínez-Sanz, M. (2021). Multifunctional cellulosic aerogels from *Posidonia oceanica* waste biomass with antioxidant properties for meat preservation. *International Journal of Biological Macromolecules, 185*, 654–663. https://doi.org/10.1016/j.ijbiomac.2021.06.192

Benito-González, I., López-Rubio, A., Gómez-Mascaraque, L. G., & Martínez-Sanz, M. (2020). PLA coating improves the performance of renewable adsorbent pads based on cellulosic aerogels from aquatic waste biomass. *Chemical Engineering Journal, 390*, Article 124607. https://doi.org/10.1016/j.cej.2020.124607

Buchtová, N., & Budtova, T. (2016). Cellulose aero-, cryo- and xerogels: Towards understanding of morphology control. *Cellulose, 23*, 2585–2595. https://doi.org/10.1007/s10570-016-0960-8

Buchtová, N., Pradille, C., Bouvard, J. L., & Budtova, T. (2019). Mechanical properties of cellulose aerogels and cryogels. *Soft Matter, 15*(39), 7901–7908. https://doi.org/10.1039/C9SM01028A

Cabrera-Villamizar, L. A., Ebrahimi, M., Martínez-Abad, A., Talens-Perales, D., López-Rubio, A., & Fabra, M. J. (2024). Order matters: Methods for extracting cellulose from rice straw by coupling alkaline, ozone and enzymatic treatments. *Carbohydrate Polymers, 328*, Article 121746. https://doi.org/10.1016/j.carbpol.2023.121746

Cabrera-Villamizar, L., Campano, C., López-Rubio, A., Fabra, M. J., & Prieto, M. A. (2024). Tailoring the structural and physicochemical properties of rice straw cellulose-based cryogels by cell-mediated polyhydroxyalkanoate deposition. *Carbohydrate Polymers, 346*, 122604. https://doi.org/10.1016/j.carbpol.2024.122604

Carlez, A., Veciana-Nogues, T., & Cheftel, J. C. (1995). Changes in colour and myoglobin of minced beef meat due to high pressure processing. *LWT - Food Science and Technology, 28*(5), 528–538. https://doi.org/10.1006/fstl.1995.0088

Castrica, M., Miraglia, D., Menchetti, L., Branciari, R., Ranucci, D., & Balzaretti, C. M. (2020). Antibacterial effect of an active absorbent pad on fresh beef meat during the shelf-life: Preliminary results. *Applied Sciences, 10*(21), 7904. https://doi.org/10.3390/app10217904

Cichosz, S., & Masek, A. (2020). IR study on cellulose with the varied moisture contents: Insight into the supramolecular structure. *Materials, 13*(20), 4573. https://doi.org/10.3390/ma13204573

Ciuffarin, F., Négrier, M., Plazzotta, S., Libralato, M., Calligaris, S., Budtova, T., & Manzocco, L. (2023). Interactions of cellulose cryogels and aerogels with water and oil: Structure-function relationships. *Food Hydrocolloids, 140*, Article 108631. https://doi.org/10.1016/j.foodhyd.2023.108631

Darpentigny, C., Nonglaton, G., Bras, J., & Jean, B. (2020). Highly absorbent cellulose nanofibrils aerogels prepared by supercritical drying. *Carbohydrate Polymers, 229*, Article 115560. https://doi.org/10.1016/j.carbpol.2019.115560

de Oliveira, J. P., Bruni, G. P., Fabra, M. J., da Rosa Zavareze, E., López-Rubio, A., & Martínez-Sanz, M. (2019). Development of food packaging bioactive aerogels through the valorization of *Gelidium sesquipedale* seaweed. *Food Hydrocolloids, 89*, 337–350. https://doi.org/10.1016/j.foodhyd.2018.10.047

Demitri, C., Del Sole, R., Scalera, F., Sannino, A., Vasapollo, G., Maffezzoli, A., Ambrosio, L., & Nicolais, L. (2008). Novel superabsorbent cellulose-based hydrogels crosslinked with citric acid. *Journal of Applied Polymer Science, 110*(4), 2453–2460. https://doi.org/10.1002/app.28660

Domínguez, R., Pateiro, M., Gagaoua, M., Barba, F. J., Zhang, W., & Lorenzo, J. M. (2019). A comprehensive review on lipid oxidation in meat and meat products. *Antioxidants, 8*(10), 429. https://doi.org/10.3390/antiox8100429

Fontes-Candia, C., Erboz, E., Martínez-Abad, A., López-Rubio, A., & Martínez-Sanz, M. (2019). Superabsorbent food packaging bioactive cellulose-based aerogels from *Arundo donax* waste biomass. *Food Hydrocolloids, 96*, 151–160. https://doi.org/10.1016/j.foodhyd.2019.05.011

Geminiani, L., Campione, F. P., Corti, C., Luraschi, M., Motella, S., Recchia, S., & Rampazzi, L. (2022). Differentiating between natural and modified cellulosic fibres

using ATR-FTIR spectroscopy. *Heritage, 5*(4). https://doi.org/10.3390/heritage5040213

Ghasemzadeh, A., Jaafar, H. Z., Juraimi, A. S., & Tayebi-Meigooni, A. (2015). Comparative evaluation of different extraction techniques and solvents for the assay of phytochemicals and antioxidant activity of hashemi rice bran. *Molecules, 20*(6), 10822–10838. https://doi.org/10.3390/molecules200610822

Gibson, K. (2006). Hemp: A substance of hope. *Journal of Industrial Hemp, 10*(2), 75–83. https://doi.org/10.1300/J237v10n02_07

Iskandar, M. A., Yahya, E. B., Abdul Khalil, H. P. S., Rahman, A. A., & Ismail, M. A. (2022). Recent progress in modification strategies of nanocellulose-based aerogels for oil absorption application. *Polymers, 14*(5), 849. https://doi.org/10.3390/polym14050849

Isogai, A., Saito, T., & Fukuzumi, H. (2011). TEMPO-oxidized cellulose nanofibers. *Nanoscale, 3*(1), 71–85. https://doi.org/10.1039/C0NR00583E

Kaur, J., Sharma, K., & Kaushik, A. (2023). Waste hemp-stalk derived nutrient encapsulated aerogels for slow release of fertilizers: A step towards sustainable agriculture. *Journal of Environmental Chemical Engineering, 11*(3), Article 109582. https://doi.org/10.1016/j.jece.2023.109582

Korhonen, O., & Budtova, T. (2020). All-cellulose composite aerogels and cryogels. *Composites Part A: Applied Science and Manufacturing, 137*, Article 106027. https://doi.org/10.1016/j.compositesa.2020.106027

Lai, H., Zhuo, H., Hu, Y., Shi, G., Chen, Z., Zhong, L., & Zhang, M. (2021). Anisotropic carbon aerogel from cellulose nanofibers featuring highly effective compression stress transfer and pressure sensing. *ACS Sustainable Chemistry & Engineering, 9*(29), 9761–9769. https://doi.org/10.1021/acssuschemeng.1c02051

Le Troedec, M., Sedan, D., Peyratout, C., Bonnet, J. P., Smith, A., Guinebretiere, R., … Krausz, P. (2008). Influence of various chemical treatments on the composition and structure of hemp fibres. *Composites Part A: Applied Science and Manufacturing, 39*(3), 514–522. https://doi.org/10.1016/j.compositesa.2007.12.001

Lee, S., Chun, S. J., Kang, I. A., & Park, J. Y. (2009). Preparation of cellulose nanofibrils by high-pressure homogenizer and cellulose-based composite films. *Journal of Industrial and Engineering Chemistry, 15*(1), 50–55. https://doi.org/10.1016/j.jiec.2008.07.008

Li, Y., Qi, B., Luo, J., Khan, R., & Wan, Y. (2015). Separation and concentration of hydroxycinnamic acids in alkaline hydrolyzate from rice straw by nanofiltration. *Separation and Purification Technology, 149*, 315–321. https://doi.org/10.1016/j.seppur.2015.06.006

Liebner, F., Potthast, A., Rosenau, T., Haimer, E., & Wendland, M. (2008). Cellulose aerogels: Highly porous, ultra-lightweight materials. *Holzforschung, 62*, 129–135. https://doi.org/10.1515/HF.2008.051

Liu, Z., Khurshid, K., & Saldaña, M. D. (2024). Hydrogels and aerogels of cellulose nanofiber derived from barley straw with addition of chitosan using high-intensity ultrasound and supercritical CO_2 drying. *Industrial Crops and Products, 216*, Article 118755. https://doi.org/10.1016/j.indcrop.2024.118755

Long, L., Weng, Y., & Wang, Y. (2018). Cellulose aerogels: Synthesis, applications, and prospects. *Polymers, 10*(6), 623. https://doi.org/10.3390/polym10060623

Lyu, P., Xia, L., Liu, X., Hurren, C., Xu, W., & Wang, X. (2023). Self-cleaning superhydrophobic aerogels from waste hemp noil for ultrafast oil absorption and highly efficient PM removal. *Separation and Purification Technology, 306*, Article 122503. https://doi.org/10.1016/j.seppur.2022.122503

Mariana, M., Alfatah, T., HPS, A. K., Yahya, E. B., Olaiya, N. G., Nuryawan, A., … Ismail, H. (2021). A current advancement on the role of lignin as sustainable reinforcement material in biopolymeric blends. *Journal of Materials Research and Technology, 15*, 2287–2316. https://doi.org/10.1016/j.jmrt.2021.08.139

Martínez-Sanz, M., Erboz, E., Fontes, C., & López-Rubio, A. (2018). Valorization of *Arundo donax* for the production of high performance lignocellulosic films. *Carbohydrate Polymers, 199*, 276–285. https://doi.org/10.1016/j.carbpol.2018.07.029

Maurya, D. K., & Devasagayam, T. P. A. (2010). Antioxidant and prooxidant nature of hydroxycinnamic acid derivatives ferulic and caffeic acids. *Food and Chemical Toxicology, 48*(12), 3369–3373.

Méndez, D. A., Schröter, B., Martínez-Abad, A., Fabra, M. J., Gurikov, P., & López-Rubio, A. (2023). Pectin-based aerogel particles for drug delivery: Effect of pectin composition on aerogel structure and release properties. *Carbohydrate Polymers, 306*, Article 120604. https://doi.org/10.1016/j.carbpol.2023.120604

Menzel, C., González-Martínez, C., Vilaplana, F., Diretto, G., & Chiralt, A. (2020). Incorporation of natural antioxidants from rice straw into renewable starch films. *International Journal of Biological Macromolecules, 146*, 976–986. https://doi.org/10.1016/j.ijbiomac.2019.09.222

Mhlongo, J. T., Nuapia, Y., Tlhaole, B., Mahlangu, O. T., & Etale, A. (2022). Optimization of hemp bast microfiber production using response surface modelling. *Processes, 10*(6), 1150. https://doi.org/10.3390/pr10061150

Mijas, G., Manich, A., Lis, M. J., Riba-Moliner, M., Algaba, I., & Cayuela, D. (2021). Analysis of lignin content in alkaline treated hemp fibers: Thermogravimetric studies and determination of kinetics of different decomposition steps. *Journal of Wood Chemistry and Technology, 41*(5), 210–219. https://doi.org/10.1080/02773813.2021.1970185

Momeni, S., Safder, M., Khondoker, M. A. H., & Elias, A. L. (2021). Valorization of hemp hurds as bio-sourced additives in PLA-based biocomposites. *Polymers, 13*(21), 3786.

Nasution, H., Harahap, H., Dalimunthe, N. F., Ginting, M. H. S., Jaafar, M., Tan, O. O. H., … Herfananda, A. L. (2022). Hydrogel and effects of crosslinking agent on cellulose-based hydrogels: A review. *Gels, 8*(9), 568. https://doi.org/10.3390/gels8090568

Nita, L. E., Ghilan, A., Rusu, A. G., Neamtu, I., & Chiriac, A. P. (2020). New trends in bio-based aerogels. *Pharmaceutics, 12*(5), 449. https://doi.org/10.3390/pharmaceutics12050449

Olszowy, M., & Dawidowicz, A. L. (2016). Essential oils as antioxidants: Their evaluation by DPPH, ABTS, FRAP, CUPRAC, and β-carotene bleaching methods. *Monatshefte Für Chemie-Chemical Monthly, 147*, 2083–2091. https://doi.org/10.1007/s00706-016-1837-0

Paulauskiene, T., Sirtaute, E., Tadzijevas, A., & Uebe, J. (2024). Mechanical properties of cellulose aerogel composites with and without crude oil filling. *Gels, 10*(2), 135. https://doi.org/10.3390/gels10020135

Pirozzi, A., Rincón, E., Espinosa, E., Donsì, F., & Serrano, L. (2023). Nanostructured cellulose-based aerogels: Influence of chemical/mechanical cascade processes on quality index for benchmarking dye pollutant adsorbents in wastewater treatment. *Gels, 9*(12), 958. https://doi.org/10.3390/gels9120958

Puangsin, B., Soeta, H., Saito, T., & Isogai, A. (2017). Characterization of cellulose nanofibrils prepared by direct TEMPO-mediated oxidation of hemp bast. *Cellulose, 24*, 3767–3775. https://doi.org/10.1007/s10570-017-1390-y

Rachini, A., Le Troedec, M., Peyratout, C., & Smith, A. (2009). Comparison of the thermal degradation of natural, alkali-treated and silane-treated hemp fibers under air and an inert atmosphere. *Journal of Applied Polymer Science, 112*(1), 226–234. https://doi.org/10.1002/app.29412

Sanchez, L. M., Hopkins, A. K., Espinosa, E., Larrañeta, E., Malinova, D., McShane, A. N., … Rodríguez, A. (2023). Antioxidant cellulose nanofibers/lignin-based aerogels: A potential material for biomedical applications. *Chemical and Biological Technologies in Agriculture, 10*(1), 72. https://doi.org/10.1186/s40538-023-00438-z

Sanchez-Salvador, J. L., Campano, C., Balea, A., Tarrés, Q., Delgado-Aguilar, M., Mutjé, P., … Negro, C. (2022). Critical comparison of the properties of cellulose nanofibers produced from softwood and hardwood through enzymatic, chemical and mechanical processes. *International Journal of Biological Macromolecules, 205*, 220–230. https://doi.org/10.1016/j.ijbiomac.2022.02.074

Šutka, A., Kukle, S., Gravitis, J., & Grave, L. (2013). Characterization of cellulose microfibrils obtained from hemp. In *Conference papers in science, 2013*. https://doi.org/10.1155/2013/171867, 189357.

Vallejo, M., Cordeiro, R., Dias, P., Moura, C., Henriques, M., Seabra, I. J., & Morouço, P. (2021). Recovery and evaluation of cellulose from agroindustrial residues of corn, grape, pomegranate, strawberry-tree fruit and fava. *Bioresources and Bioprocessing, 8*(1), 1–12.

Vârban, R., Crișan, I., Vârban, D., Ona, A., Olar, L., Stoie, A., & Ștefan, R. (2021). Comparative FT-IR prospecting for cellulose in stems of some fiber plants: Flax, velvet leaf, hemp and jute. *Applied Sciences, 11*(18), 8570. https://doi.org/10.3390/app11188570

Wang, H. D., & Kim, J. (2022). Citric acid-crosslinked highly porous cellulose nanofiber foam prepared by an environment-friendly and simple process. *Global Challenges, 6*(11), Article 2200090. https://doi.org/10.1002/gch2.202200090

Wang, X., Yang, X., Wu, Z., Liu, X., Li, Q., Zhu, W., … Hu, L. (2023). Enhanced mechanical stability and hydrophobicity of cellulose aerogels via quantitative doping of nano-lignin. *Polymers, 15*(5), 1316. https://doi.org/10.3390/polym15051316

Wu, W., Zhou, Y., Pan, J., Wu, Y., Goksen, G., & Shao, P. (2023). Multibranched flower-like ZnO anchored on pectin/cellulose nanofiber aerogel skeleton for enhanced comprehensive antibacterial capabilities. *Carbohydrate Polymers, 322*, Article 121320. https://doi.org/10.1016/j.carbpol.2023.121320

Wu, Y., Wu, W., Farag, M. A., & Shao, P. (2023). Functionalized cellulose nanocrystal embedded into citrus pectin coating improves its barrier, antioxidant properties and potential application in food. *Food Chemistry, 401*, Article 134079. https://doi.org/10.1016/j.foodchem.2022.134079

Yang, T., Wang, J., Li, B., Kai, X., Xing, W., & Li, R. (2018). Behaviors of rice straw two-step liquefaction with sub/supercritical ethanol in carbon dioxide atmosphere. *Bioresource Technology, 258*, 287–294. https://doi.org/10.1016/j.biortech.2018.02.037

Yang, X., & Cranston, E. D. (2014). Chemically cross-linked cellulose nanocrystal aerogels with shape recovery and superabsorbent properties. *Chemistry of Materials, 26*(20), 6016–6025. https://doi.org/10.1021/cm502873c

Zaman, A., Huang, F., Jiang, M., Wei, W., & Zhou, Z. (2020a). Preparation, properties, and applications of natural cellulosic aerogels: A review. *Energy and Built Environment, 1*(1), 60–76. https://doi.org/10.1016/j.enbenv.2019.09.002

Zaman, A., Huang, F., Jiang, M., Wei, W., & Zhou, Z. (2020b). Preparation, properties, and applications of natural cellulosic aerogels: A review. *Energy and Built Environment, 1*(1), 60–76. https://doi.org/10.1016/j.enbenv.2019.10.002

Zhang, X., Yu, Y., Jiang, Z., & Wang, H. (2015). The effect of freezing speed and hydrogel concentration on the microstructure and compressive performance of bamboo-based cellulose aerogel. *Journal of Wood Science, 61*, 595–601. https://doi.org/10.1007/s10086-015-1514-7

Zheng, Q., Tian, Y., Ye, F., Zhou, Y., & Zhao, G. (2020). Fabrication and application of starch-based aerogel: Technical strategies. *Trends in Food Science & Technology, 99*, 608–620. https://doi.org/10.1016/j.tifs.2020.03.038

Zhu, J., Zhu, Y., Ye, Y., Qiu, Z., Zhang, Y., Yu, Z., … Jiang, F. (2023). Superelastic and ultralight aerogel assembled from hemp microfibers. *Advanced Functional Materials, 33*(22), Article 2300893. https://doi.org/10.1002/adfm.202300893

Zhu, W., Zhang, Y., Wang, X., Wu, Y., Han, M., You, J., Xu, F., & Kim, J. (2022). Aerogel nanoarchitectonics based on cellulose nanocrystals and nanofibers from eucalyptus pulp: Preparation and comparative study. *Cellulose, 29*(2), 817–833. https://doi.org/10.1007/s10570-021-04294-8